Solution Structure of a RNA Decamer Duplex, Containing 9-[2-*O*-(*β*-D-ribofuranosyl)-*β*-D-ribofuranosyl]adenine, a Special Residue in Lower Eukaryotic Initiator tRNAs

by **Ingrid Luyten**[a]), **Robert M. Esnouf**[a]), **Sergey N. Mikhailov**[b]), **Ekaterina V. Efimtseva**[b]), **Paul Michiels**[c]), **Hans A. Heus**[c]), **Cees W. Hilbers**[c]), and **Piet Herdewijn**[a])*

[a]) Rega Institute for Medical Research, K. U. Leuven, Minderbroedersstraat, 10, B-3000 Leuven
[b]) Engelhardt Institute of Molecular Biology, Russian Academy of Sciences, Vavilov Str. 32, Moscow, 117984, Russia
[c]) Nijmegen SON Research Center for Molecular Structure, Design and Synthesis, Laboratory of Biophysical Chemistry, Universiteit Nijmegen, Toernooiveld, NL-6525 ED Nijmegen

The solution structure of the self-complementary deca-ribonucleotide 5′-r(GCGA*AUUCGC)-3′ containing 9-[2-*O*-(*β*-D-ribofuranosyl)-*β*-D-ribofuranosyl]adenine (A*), a modified nucleotide that occurs in lower eukaryotic methionine initiator tRNAs ($tRNAs_i^{Met}$), was determined by NMR spectroscopy. Unexpectedly, the modification has no effect on the thermal stability of the duplex. However, the extra ribose moiety is in the C(3′)-*endo* conformation and takes up a well-defined position in the minor groove, which is in agreement with its position in $tRNAs_i^{Met}$ as determined by X-ray crystallography. Molecular-dynamics simulations on the RNA duplex in H_2O show that the position of the extra ribofuranose moiety seems to be stabilized by bridged H-bonds (mediated by two H_2O molecules) to the backbone of the complementary chain.

Introduction. – Oligonucleotides that hybridize sequence-specifically with mRNA can be used to control gene expression, providing that they are stable against enzymatic degradation and that they bind with high affinity to their RNA targets. Such molecules are termed antisense oligonucleotides. They can function by a variety of mechanisms, including *i*) translation arrest by blocking the progression of the ribosome and *ii*) inactivation of the mRNA by RNase H cleavage. The stability of the duplex formed between the antisense oligonucleotide and its RNA target can be influenced by introducing chemical modifications into the antisense strand. One of the simplest modifications is the introduction of an alkoxy group at the 2′-position in the deoxyribose moiety of oligodeoxyribonucleotides [1]. It has been demonstrated that 2′-*O*-alkyl-RNA·RNA hybrids where the alkyl group has the general structure $ROCH(R')CH_2$ show increased thermal stabilities when compared with duplexes containing simple alkyl groups such as propyl or allyl [1]. An alkyl group of the general structure $ROCH_2$ has no beneficial effect on the stability of the duplex when compared with the equivalent dsRNA sequence. DNA with the analogous 2′-(2-methoxyethoxy) substituent ($MeOCH_2CH_2O$) is currently undergoing extensive biological evaluation as an antisense construct. *Freier* and *Altmann* [2] have hypothesized that, due to the *gauche* effect between the O-atoms of the methoxyethoxy substituent, the conformation of the side chain is restricted and consistent with *A*-form duplex formation. Generally speaking, a $XCH(R)CH_2O$ substituent at C(2′) may stabilize the duplex when X is an electronegative group and R is any group from the series H, Me, $HOCH_2$, or $MeOCH_2$. Recently, it has been found by X-ray diffraction methods [3] that, in some

structures of DNA duplexes with incorporated 2′-*O*-modified RNA analogues, a H_2O molecule can coordinate between the phosphate backbone and the O-atoms of the 2′-*O*-(methoxyethyl) substituent.

To avoid an entropic penalty during duplex formation, it could be reasoned that the 2′-*O*-alkoxyethyl substituent should be replaced by a conformationally more rigid substituent. A good candidate for this might be a sugar substituent such as a ribosyl unit. Furthermore, the free OH groups of the 2′-*O*-ribosyl substituent might influence hydration of the duplex in a similar manner as described above. On the other hand, a 2′-*O*-ribosyl substituent is much larger than a 2′-*O*-(methoxyethyl) substituent, and interaction of the ribosyl substituent with minor-groove functionalities might disrupt base pairing for steric reasons. Interestingly, this kind of modification is also present in tRNA [4]. The disaccharide nucleosides 9-[2-*O*-(*β*-D-ribofuranosyl)-*β*-D-ribofuranosyl]-adenine (A*) (*Fig. 1*) and 9-[2-*O*-(*β*-D-ribofuranosyl)-*β*-D-ribofuranosyl]guanine (G*) can bear additional phosphate esters at their 2′-*O*-ribosyl moieties. These modifications occur in lower eukaryotic methionine initiator tRNAs ($tRNAs_i^{Met}$ [4]), where they are present at position 64, which is located near the junction of the T-stem and the aminoacyl stem in the tRNA tertiary structure. It was suggested that this modification might act as a discriminator for the elongation-initiator process [5] in preventing the $tRNAs_i^{Met}$ from participating in the elongation cycle. A 3-Å crystal structure [6] of a $tRNA_i^{Met}$ showed that this modification lies in the minor groove with the 5′*-phosphate group interacting with $NH_2-C(2)$ of the neighboring G63. However, the exact position of the individual atoms of this 2′-*O*-ribosyl moiety could not be specified because of insufficient resolution. Therefore, the study of a simpler RNA structure with this disaccharide-containing nucleotide by NMR spectroscopy and restrained molecular dynamics may provide more insight into the structural features of these $tRNAs_i^{Met}$. We have chosen as a model a modification of the already described [7] self-complementary oligoribonucleotide sequence 5′-r(GCGAAUUCGC)-3′, in which A4 is replaced by A*, *i.e.*, 5′-r(GCGA*AUUGC)-3′. This model preserves a neighboring G on the 5′ side of A*, as in the $tRNA_i^{Met}$ structure.

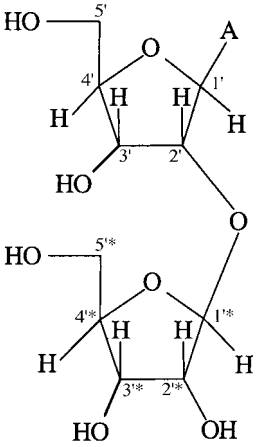

Fig. 1. *The disaccharide nucleoside 9-[2-*O*-(β-*D*-ribofuranosyl)-β-*D*-ribofuranosyl]adenine* (A*). To avoid confusion between the two sugar rings in A*, the extra ribose moiety has starred locants.

Experimental. – *Sample Preparation*. The phosphoramidite of the modified nucleoside (A*) was used for solid-phase RNA synthesis, as described before [8]. The self-complementary oligoribonucleotide 5′-r(GCGA*AUUCGC)-3′ containing 9-[2-*O*-(β-D-ribofuranosyl)-β-D-ribofuranosyl]adenine (A*) was purchased from *Eurogentec*. The total yield was *ca*. 9 mg of RNA.

Melting Temperatures. Oligomers were dissolved in a buffer containing 0.1M NaCl, 0.02M potassium phosphate (pH 7.5), and 0.1 mM EDTA. Concentrations were determined to be *ca*. 4 μM by measuring the absorbance at 260 nm at 80°. The following extinction coefficients (ε) were used: A and A*, 15000; U, 10000; G, 12500; C, 7500. Melting curves were determined with a *Uvikon-940* spectrophotometer. Cuvette temp. was controlled by water circulation through the cuvette holder. The temp. of the soln. was measured with a thermistor directly immersed in the cuvette. Temp. control and data acquisitions were carried out automatically with an IBM-compatible computer. The samples were heated and cooled at a rate of 0.5° min^{-1}. Melting temp. were derived from the first derivative of the absorbance *vs.* temperature curves.

NMR Spectroscopy. NMR Samples were prepared by dissolving the purified RNA (*ca*. 9 mg) in D_2O and adjusting the pD to 6.8 with DCl. The sample was divided in two parts and lyophilized. One part was dissolved in D_2O (0.750 ml), and the other part was dissolved in D_2O (0.075 ml) and H_2O (0.675 ml). The samples were annealed by heating to 80° followed by slow cooling to obtain a 1.8 mM concentration of the duplex.

NMR Spectra: *Varian-500 Unity* spectrometer; at 499.505 MHz unless stated otherwise; δ in ppm, *J* in Hz. Quadrature detection was achieved by the *States-Haberkorn* hypercomplex mode [9]. Spectra were processed with the programs NMRPipe [10] and XEASY [11] running on a *Silicon-Graphics-O2* workstation (IRIX version 6.3).

The 1D- and 2D-NOESY experiments from the sample dissolved in H_2O/D_2O 9:1 were recorded at 5° (*Varian Unity*(+)-*500* spectrometer, at 499.930 MHz), using a jump-return sequence as the observation pulse [12]. Sweep widths of 10000 Hz in both dimensions were used with 64 scans, 2048 data points in t_2 and 512 FIDs in t_1. The data were apodized with a shifted sine-bell square function in both dimensions and processed to a $4K \times 2K$ matrix. The 2D DQF-COSY [13], TOCSY [14], and NOESY [15] spectra from the sample in D_2O were recorded with sweep widths of 5000 Hz in both dimensions. The residual HDO peak was suppressed by presaturation. The ^{31}P-decoupled DQF-COSY spectrum consisted of 4096 datapoints in t_2 and 400 increments in t_1. The data were apodized with a shifted sine-bell square function in both dimensions and processed to a $4K \times 2K$ matrix. For the TOCSY experiment, a Clean MLEV17 [16] version was used, with a low-power 90° pulse of 26.6 μs and the delay set to 69.2 μs. The total TOCSY mixing time was set to 65 ms. The spectrum was acquired with 32 scans, 4096 data points in t_2 and 256 FIDs in t_1. The data were apodized with a shifted sine-bell square function in both dimensions and processed to a $4K \times 1K$ matrix. The NOESY experiments were acquired with mixing times of 50, 100, 150, 250, and 300 ms, 64 scans, and 2048 datapoints in t_2 and 512 increments in t_1.

A ^{1}H,^{31}P-HETCOR [17] was acquired (*Varian Unity(+)-500* spectrometer, at 499.930 MHz) with 32 scans, 4096 data points in the ^{1}H dimension, t_2, and 400 real data points in the ^{31}P dimension, t_1, over sweep widths of 5000 and 2000 Hz, resp.

Restraint Generation and Refinement Procedures. Interproton-distance restraints were derived from cross-peak volumes in the 50, 100, and 150 ms NOESY spectra and were given ±20% error bounds. Cross-peaks that were only observable with longer mixing times were corrected for spin diffusion by using the H−C(5)/H−C(6) NOE (2.45 Å) as a reference for shorter distances and helical intraresidue H−C(1′)/H−C(6) or H−C(8) NOEs (3.65 Å) for longer distances [18]. All NOEs that could not be properly integrated because of overlap were assigned bounds of 1.8 to 7.0 Å. This resulted in 55 inter- and 110 intra-residue distance restraints. Conservative imino/imino (4.0 Å), imino H−C(1′) (5.0 Å) and imino H−C(2) (2.9 Å) distance restraints were obtained from the spectrum in H_2O and included in the structure calculations. H-Bond restraints were used and treated as NOE restraints to define the *Watson-Crick* base pairing. All residues (except C10) in the RNA strand gave no observable H−C(1′)/H−C(2′) cross-peaks in the DQF-COSY experiment. Therefore, dihedral restraints on H−C(1′)−C(2′)−H (99 ± 20°) and H−C(2′)−C(3′)−H (38 ± 20°) were used to constrain the *N*-type ribose conformation [19]. All structure calculations were performed with X-PLOR V3.851 [20]. The standard topology and parameter files were adapted for the extra 2′-*O*-ribose moiety. The torsion-angle dynamics protocol used was largely identical to that implemented for a DNA duplex [21], starting from an extended strand conformation and proceeding in four stages. *i*) A 60 ps (4000 steps of 15 fs) high-temperature torsion-angle molecular dynamics (TAMD) (simulation temp. of 20000 K) with a decreased weight on the repulsive nonbonded energy term ($\omega_{vdw} = 0.1$) to facilitate crossing rotational-energy barriers, and coefficients for the dihedral and the NOE energy terms of 5 ($\omega_{dihedral}$) and 150 (ω_{NOE}), respectively. *ii*) A 90 ps (6000 steps of 15 fs) slow cooling TAMD (from 20000 to 1000 K) with the ω_{vdw} gradually increasing to 1.0. *iii*) A 9 ps (3000 steps of

3 fs) cartesian molecular dynamics (cooling from 1000 to 300 K). *iv*) A 1000-step conjugate-gradient-energy minimization with $\omega_{dihedral} = 200$ and $\omega_{NOE} = 50$. Out of 100 calculated structures, 24 had no NOE-distance violations (> 0.5 Å) and no dihedral-angle violations (> 5°) (*Table 1*). The residual average violations were 0.091 Å and 0.7°, respectively. From the 24 structures, the 10 structures closest to the average of all 24 were used for further analysis with the program Curves 5.1. [22].

Table 1. *Structural Statistics of the Final Set of 24 Structures of the [5′-r(GCG A*AUUCGC)]$_2$ Duplex*

	Residues 3 – 5/16 – 18	All
Restraint Violations: NOE violations > 0.5 Å	0	0
dihedral violations > 5°	0	0
Rms Deviations: from distance restraints [Å]	0.124 ± 0.021	0.091 ± 0.012
from dihedral restraints [°]	0.7 ± 0.4	0.7 ± 0.1
from idealized geometry		
Bonds [Å]	0.0107 ± 0.0001	0.0107 ± 0.0001
Angles [°]	1.247 ± 0.022	1.169 ± 0.016
Impropers [°]	0.693 ± 0.035	0.877 ± 0.016
Pairwise rmsd for all heavy atoms [Å]	0.08	0.59

Hydration Analysis. Water molecules were included using the TIP3P force field, and molecular-dynamics simulations and energy minimizations were performed using X-PLOR V3.851 [20]. A well-equilibrated cube of H_2O molecules (125 molecules in a cube of 15.55 Å) was copied and translated many times in all three dimensions to create a cube sufficiently large to embed the RNA duplex. Thus, application of periodic boundary conditions will not give rise to spurious interactions between duplexes. The RNA duplex was placed in the center of the box, and all H_2O molecules overlapping with the RNA duplex (within 2.6 Å) were removed, which led to a total of 9000 H_2O molecules. Simulations were performed with a time step of 1 fs, and the limits for nonbonded *van der Waals* and electrostatic interactions were truncated at 12 Å. The same TIP3P force field was used for the RNA duplex supplemented with the restraints derived from the NMR data. An initial equilibration simulation of 10 ps at 300 K was performed with the RNA-duplex conformation rigidly constrained, both to lose the periodicity in the H_2O structure and to allow a reasonable H_2O structure to form around the duplex. Further simulations were performed with the RNA unconstrained (a total of 20 ps starting with a simulation temp. of 500 K and reducing it to 300 K). Individual snapshots taken during this simulation were subjected to a short energy minimization and analyzed with MidasPlus [23].

Molecular Graphics. Molecular graphics images were produced with MidasPlus [23] and Rasmol [24]. *Figs. 3* and *5* were drawn with Bobscript [25], and *Fig. 5* was produced with Raster3D [25b].

Results. – *Thermal Stability of the RNA Duplex*. Melting-temperature determinations demonstrated that the thermal stabilities of oligo r(A)$_{13}$ · r(U)$_{13}$ (T_m 15.2°) and the fully modified oligo r(A*)$_{13}$ · r(U)$_{13}$ (T_m 15.2°) are equal within experimental error, implying that the extra sugar moieties have no effect on the stability of the RNA duplex. This unexpected result initiated the structural studies aimed at gaining insight into the position of the 2′-*O*-ribose moieties in the RNA duplex to understand why the modified nucleotide A* has no influence on the stability of a RNA duplex. Since the determination of the solution structure of a complex between oligo-U and fully modified oligo-A* (where A* represents the disaccharide nucleotide) is very complex, we have incorporated a single A* (= 9-[2-*O*-(*β*-D-ribofuranosyl)-*β*-D-ribofuranosyl]-adenine) unit into the well-described self-complementary oligoribonucleotide sequence [5′-r(GCGAAUUCGC)-3′]$_2$ [7] (T_m 53°). In agreement with our previous observation, the melting point of the modified double-stranded RNA [5′-r(GCGA*AUUCGC)-3′]$_2$ in 0.1M NaCl is identical to that found for the unmodified dsRNA duplex (T_m 53°). Determination of the solution structure of this modified duplex was done by a

combination of high-resolution NMR spectroscopy and restrained molecular dynamics.

^1H and ^{31}P Assignments. Resonance assignment followed standard NMR methods [19]. Sequential connectivities were established following an anomeric to aromatic proton walk (*Fig. 2*). The H–C(2′) and H–C(3′) protons were assigned through H–C(2′)/H–C(3′)/aromatic H NOE connectivities. NOESY Experiments with short mixing times (50 ms) were used for H–C(2′) assignments since the internucleotide H–C(2′)/aromatic H NOEs and the intranucleotide H–C(1′)/H–C(2′) NOEs are strong. The ^{1}H,^{31}P HETCOR [17] was acquired to confirm assignment of the H–C(3′) resonances and, when possible, the H–C(4′) and H–C(5′) resonances. The rest of the sugar spin systems could be determined by a combination of DQF-COSY, TOCSY, and NOESY experiments (*Table 2*), suggesting an *A*-form helix and stacking of the A*4 and A5 bases. The COSY cross-peak pattern clearly shows that the extra ribose moiety of A* adopts a C(3′)-*endo* conformation.

The H–C(2)(A*4) and H–C(2)(A5) protons were distinguished from other base protons by their NOEs to H–C(1′) protons. The H–C(2)(A*4) exhibits NOEs to H–C(1′)(A*), H–C(1′)(A5), and H–C(1′)(C8),

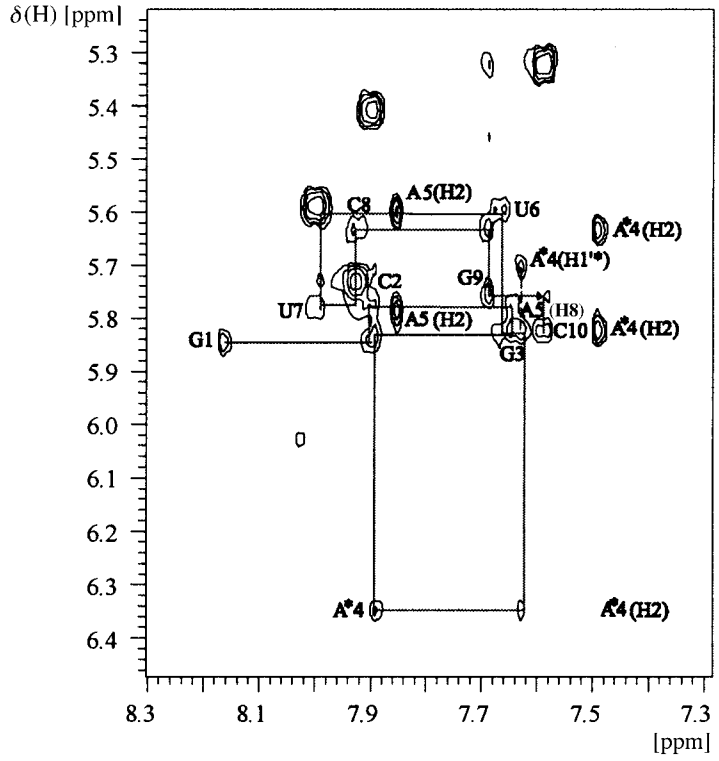

Fig. 2. *Portion of the 2D NOESY* (D_2O, 250 ms mixing time, 20°) *of [5′-r(GCG*AUUCGC)-3′]$_2$* (see *Fig. 1* for A*) *showing the aromatic to H–C(1′) region.* The sequential walk along the H–C(1′) and aromatic H–C(6)/H–C(8) protons in the RNA strand is traced out by the continuous line. Assignment of the cross-peaks: H–C(8)(A5)/H–C(1′*)(A*4) (=A5(H8)/A*4(H′*)) and H–C(1′)(A5)/H–C(8)(A5) (=A5(H1′)/A5(H8)) are indicated by the broken line.

Table 2. *Chemical Shift [ppm] Assignments for the Nonexchangeable ^{1}H-NMR Resonances in the [5′-r(GCGA*AUUCGC)-3′]$_2$-Duplex at 20°*. Referenced to the H_2O resonance at 4.86 ppm.

	H−C(1′) (= H1′)	H−C(2′) (= H2′)	H−C(3′) (= H3′)	H−C(4′) (= H4′)	H−C(5′) (= H5′)	H′−C(5) (= H5″)	H−C(8)/ H−C(6) (= H8/H6)	H−C(2)/ H−C(5) (= H2/H5)	P[a])
G1	5.84	4.90	4.66	4.48	4.13	4.01	8.16		−0.45
C2	5.77	4.78	4.67	4.58	4.63	4.32	7.90	5.41	0.07
G3	5.82	4.70	4.70	–	4.57	4.26	7.64		−0.43
A*4	6.35	4.95	4.84	4.56	4.42	4.66	7.90	7.47	−0.60
	(5.70)[b])	(4.39)[b])	(4.55)[b])	(4.20)[b])	(4.16)[b])	(3.89)[b])			
A5	5.83	4.58	4.43	4.44[c])	4.43[c])	4.22	7.64	7.84	−0.59
U6	5.60	4.57	4.53	4.58	4.64	4.14	7.67	5.03	−0.93
U7	5.78	4.59	4.60	4.53	4.63	4.19	7.99	5.59	−0.61
C8	5.63	4.54	4.58	4.49	4.62	4.21	7.92	5.73	−0.34
G9	5.75	4.46	4.66	4.51	4.64	4.17	7.69		−0.56
C10	5.83	4.06	4.25	4.25	4.56	4.11	7.59	5.32	

[a]) P-Assignments are to the 5′-nucleoside. [b]) Assignments of the equivalent sugar protons of the extra ribose moiety. [c]) Tentative assignments.

whereas H−C(2)(A5) exhibits NOEs to H−C(1′)(A5), H−C(1′)(U6), and H−C(1′)(U7), as expected for an *A*-form helix. Both H−C(2)(A*4) and H−C(2)(A5) exhibit NOEs to H−C(2)(A5) suggesting that the A*4 and A5 bases are stacked. The resonance assignment of the modified nucleotide A* was based on the resonance assignment of the monomer [8]. The H−C(1′)(A*4) proton resonates most downfield (6.35 ppm). The resonance of H−C(1′*) from the extra ribose moiety was assigned from the NOEs to H−C(1′)(A*4) (*Table 3*, 3.5 Å) and H−C(8)(A5) (see *Fig. 2*, dashed line). The rest of the sugar-proton resonances of this extra ribose moiety could then easily be assigned on the basis the NOEs to this H−C(1′*). Furthermore, in the COSY experiment, strong cross-peaks are observed for H−C(2′*)/H−C(3′*) ($^3J(2',3') \approx 5$ Hz), H−C(3′*)/H−C(4′*) ($^3J(3'*,4'*) \approx 10$ Hz), and H−C(4′*)/H−C(5′*) and H′−C(5′*) ($^3J(4'*,5'*) \approx 8$ Hz).

Table 3. *Key Distance Restraints* [Å] *for Residue A* in the [5′-r(GCG A*AUUCGC)-3′]$_2$ Duplex*

Proton 1	Proton 2	Distance		
		Lower	Upper	Distance[a])
H−C(1′)(A*4)	H−C(1′*)(A*)	2.6	3.8	3.5
H−C(1′)(A*4)	H−C(2′*)(A*4)	3.8	5.6	4.4
H−C(1′)(A*4)	H−C(3′*)(A*4)	2.6	4.0	4.0
H−C(1′*)(A*4)	H−C(2′*)(A*4)	2.2	3.3	2.8
H−C(1′*)(A*4)	H−C(2′*)(A*4)	1.9	2.9	2.5
H−C(1′*)(A*4)	H−C(4′*)(A*4)	2.7	3.9	3.3
H−C(1′)(A*4)	H−C(5′*)(A*4)	2.4	3.6	2.6
H−C(8)(A5)	H−C(1′*)(A*4)	3.5	5.3	4.1

[a]) Measured distance in the RNA duplex model, which is one of the 24 selected structures as depicted in *Fig. 5,a.*

Imino-proton assignments were based on a NOESY spectrum measured at 5° in H_2O/D_2O 9:1. The H−N(3)(U6) and H−N(3)(U7) have strong NOEs with each other and with H−C(2)(A5) and H−C(2)(A*4), respectively, as expected for an *A*-form helix. These connectivities show standard *Watson-Crick* base-pairing for A*4 and A5 and normal base stacking for U6 and U7. The H−N(1)(G3) and H−N(1)(G9)

protons show the normal cross-strand connectivities with the amino protons and H−C(5) of C8 and C2, respectively.

All assignments of the ^{31}P-resonances (*Table 1*) were derived from the 2D ^{1}H-detected ^{1}H,^{31}P-correlation spectrum (HETCOR).

NOE Distances, Sugar Puckers, and Backbone Torsions. With nearly complete ^{1}H- and ^{31}P-assignments, sufficient distances and torsion angles were determined to calculate a structure for the modified RNA duplex [5′-r(GCGA*AUUCGC)-3′]$_2$. The details of the refinement protocol are given in the *Exper. Part*.

Distance Restraints. Interproton distance restraints were derived from cross-peak volumes in 50, 100, and 150-ms NOESY spectra and were given ±20% error bounds. This resulted in 55 inter- and 110 intra-residue distance restraints. From the spectrum in H_2O, imino/imino, imino/H−C(1′) and imino/H−C(2) distance restraints were included in the structure calculations. H-Bond restraints were used and treated as NOE restraints.

Conformation of Ribose Rings in RNA. The conformation of the furanose ring can be described by the pseudorotation angle (P) and the puckering amplitude (Ψ_m). These are related to the endocyclic torsion angles that, in turn, are correlated to the vicinal ^{1}H,^{1}H-coupling constants *via* the *Karplus* equation. The combination of the small coupling constants J(1′,2′) (extremely sharp anomeric signals and no visible cross-peaks in J-correlated spectra) and the large J(3′,4′) (*ca.* 10 Hz) in the ribose moieties, is very characteristic of *N*-type sugars [19].

Backbone Dihedral-Angle Restraints. In an RNA strand, the backbone dihedral angle δ is correlated with the sugar puckering. In the *N*-type sugars, this dihedral angle is restrained to $80 \pm 20°$. The small passive couplings in the H−C(5′)/H′−C(5′) cross-peaks of the DQF-COSY experiment allowed the backbone dihedral angles γ to be restrained in the RNA strand to $60 \pm 35°$. The ε backbone dihedral angles were restrained to $-130 \pm 40°$, based on the large J(P,3′) (*ca.* 11 Hz) measured in the ^{1}H,^{31}P-HETCOR spectrum. The lack of P/H−C(5′) and P/H′−C(5′) cross-peaks in this spectrum is an indication of small J(P,5′) and J(P,5″) coupling constants which correspond to the β backbone dihedral angles having a *trans* conformation ($180 \pm 30°$). The ^{31}P-chemical shift was used to constrain the α and ζ backbone dihedral angles within the region $0 \pm 120°$.

Structure Determination and Analysis. Starting from two extended strands, a set of 100 structures was generated by torsion-angle molecular dynamics (*cf. Exper. Part*). Out of 100 calculated structures, 24 were selected for analysis that had no NOE-distance violations > 0.5 Å and no dihedral-angle violations $> 5°$. The residual average violations were 0.091 Å and 0.7°, respectively. Superimpositions were made for all heavy atoms of base pairs 3–5/16–18 on one side of the duplex for the 24 structures. *Fig. 3* shows the models after superimposition of the ten selected structures closest to the average. The part of the duplex around the modified adenosine (*Fig. 3*,*c*) is well-defined because of the high number of restraints per residue as well as for the extra ribose ring, but the precision is lost progressively going away from this part of the molecule as a result of the lack of long-range distance restraints in the structure determination of RNA helices by NMR [26]. The local superimposition of the domain 3–5/16–18 containing the modified adenosine yields a root mean square deviation (rmsd) of 0.08 Å, whereas the global rmsd gives a value of 0.59 Å (*Table 1*).

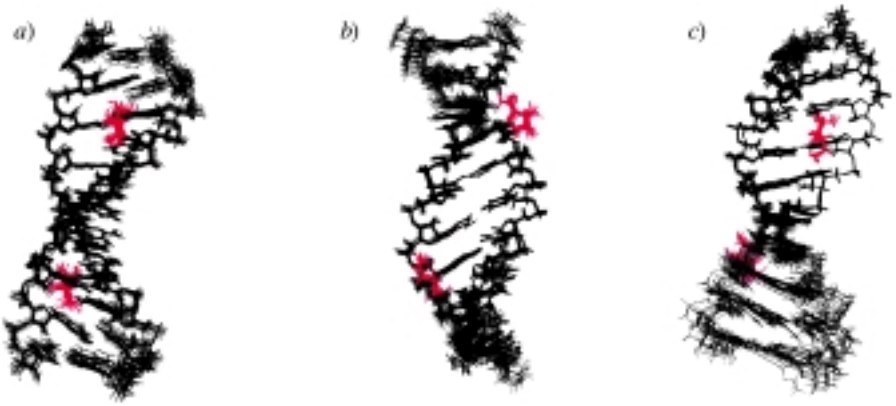

Fig. 3. *Views of the three-dimensional structure of the RNA structure modified with 9-[2-O-(β-D-ribofuranosyl)-β-D-ribofuranosyl]adenine* (A*). a) *All heavy atom superimposition of the ten structures closest to the average of the 24 final structures.* b) *The same superimposition rotated by 90 degrees.* c) *Overlays of the same ten structures, but the superimposition is limited to the heavy atoms in the residues 3–5/16–18.*

The precision in the definition of these structures is further evidenced by the small variation in the torsion angles (*Fig. 4*), shown for the 10 selected structures closest to the average. The values also correspond to a helix with an *A*-type conformation.

Orientation and Conformation of the Extra Ribose Ring. The extra ribose ring has a fixed orientation in the minor groove (*Fig. 5* shows a part of the structure around the modification of one of the 24 selected structures) and adopts a C(3′)-*endo* conformation. The latter can be deduced from the lack of an observable H−C(1′*)/H−C(2′*) cross-peak in the DQF-COSY and because $J(3'^*,4'^*)$ is *ca.* 10 Hz. We have used the three-bond ^{1}H,^{1}H coupling constants, *i.e.*, $^3J(2'^*,3'^*) \approx 5$ Hz and $^3J(3'^*,4'^*) \approx 10$ Hz to restrain the δ dihedral angle to $80 \pm 20°$, as found in a C(3′)-*endo* conformation. In the free disaccharide nucleoside (*i.e.*, monomeric A*) [8], the extra ribose moiety also adopts a C(3′)-*endo* conformation. The observed $J(4'^*, 5'^*)$ of *ca.* 8 Hz corresponds to mixed populations of *gauche* and *trans* rotamers of the C(4′*)−C(5′*) bond. Therefore, we have not restrained this γ dihedral angle.

The key NOEs, shown in *Table 3*, lead to an orientation of the 2′-*O*-ribose moiety as depicted in *Fig. 5*. The O(2′)−C(1′*)−C(2′*)−O(2′) torsion angle is roughly $-134°$, and the extra ribose moiety is oriented more or less perpendicular to the plane of the A*·U6 base pair and more or less perpendicular to the A* ribose such that H−C(5′*) and H−C(1′*) are only 2.6 Å apart, whereas the H−C(3′*) and the H−C(1*) are separated by roughly 4 Å. H−C(1′*) points in the direction of A5 and is only 4.1 Å away from H−C(8)(A5).

Discussion. – This NMR study reveals that the duplex RNA substituted with one 9-[2-*O*-(β-D-ribofuranosyl)-β-D-ribofuranosyl]adenine (A*) [8] maintains an *A*-type helical geometry and that the modified adenosine has no profound effect on the RNA structure when paired opposite to a uridine residue and stacked between two other purine nucleotides. Nevertheless, the extra sugar ring does take

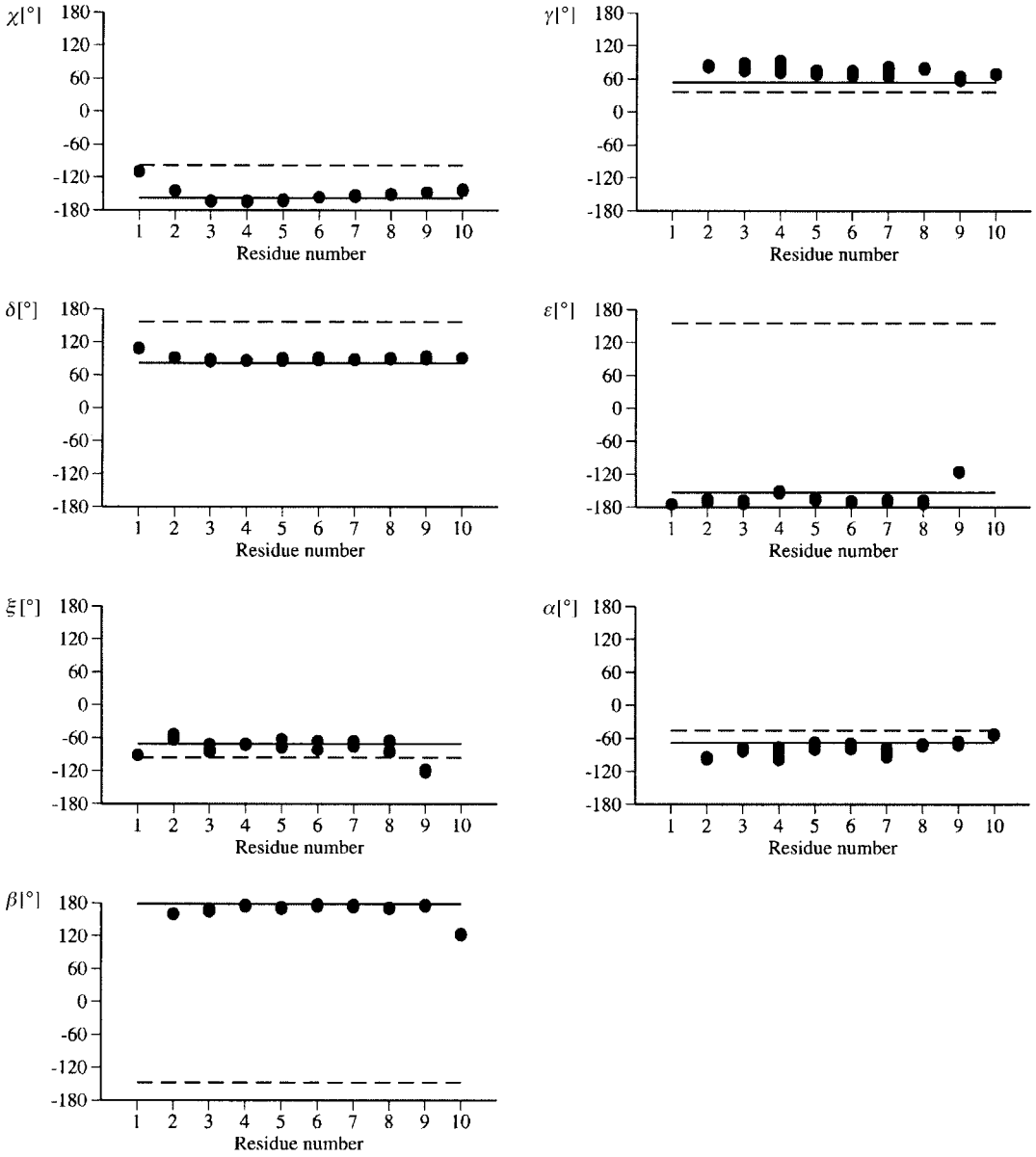

Fig. 4. *Variation of the torsion angles for the individual residues of the 10 structures. A*- and *B*-form values are given by dashed and dotted lines, respectively.

up a well-defined position in the minor groove, as illustrated in *Fig. 5*, which is in agreement with the X-ray data [6] of $tRNAs_i^{Met}$ where the extra sugar moiety is placed in the minor groove with its 5′-phosphate group pointing to $NH_2-C(2)$ of the neighboring 5′-G residue. *Fig. 5,b* shows that the distances between $NH_2-C(2)$ of G3 and O(5′*) of A*4 and between O(2′*) of A*4 and O(4′) of A5 are within H-bond

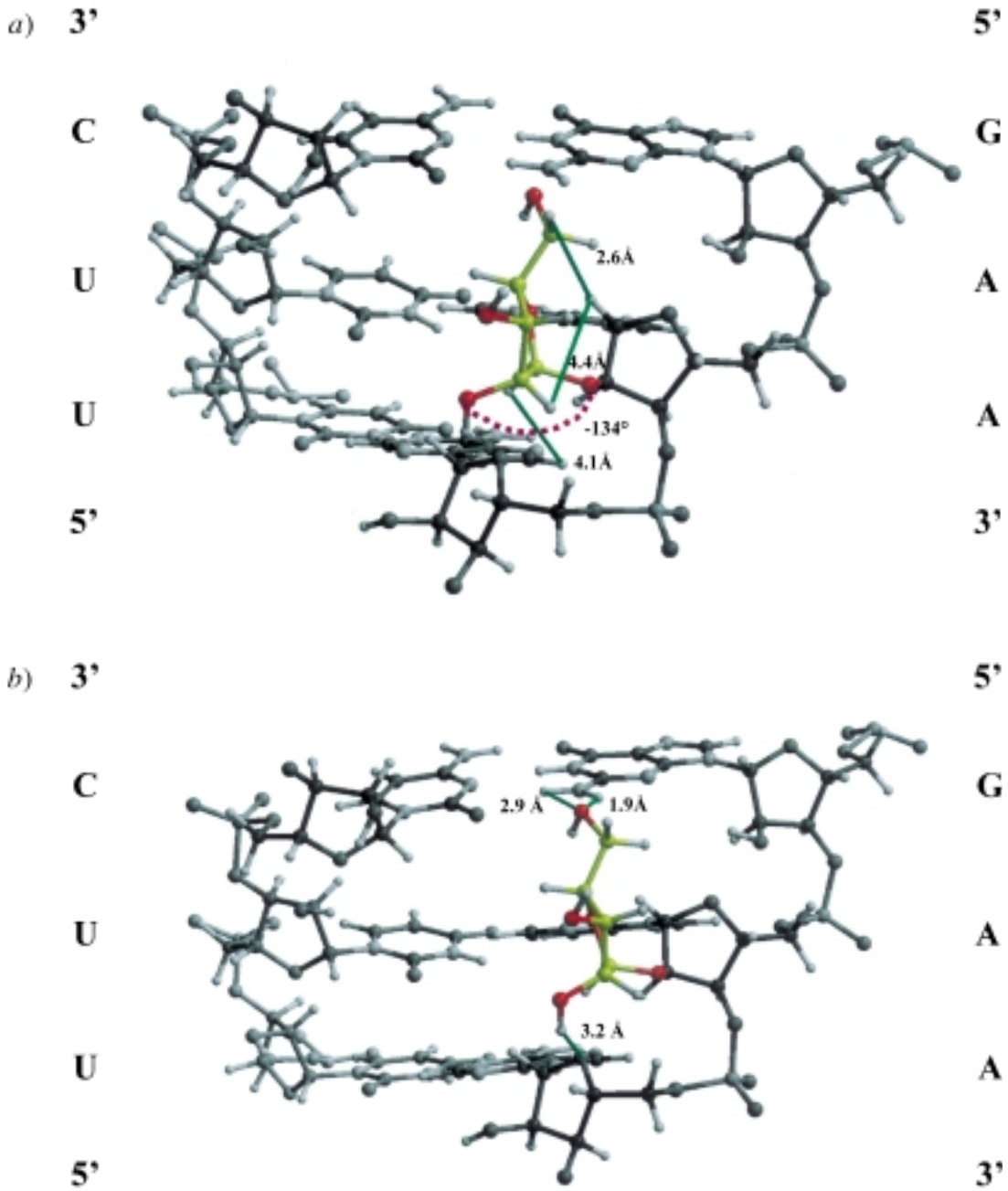

Fig. 5. a) *View of a part of the duplex around the modified residue of one of the selected RNA structure showing key distances as green lines.* b) *View a) slightly rotated to point out the possible H-bonds* ((A*4)O(5′*)···H(21)–N(2)(G3) or (A*4)(O5′*)···H(22)–N(2)(G3) and/or (A*4)O(2′*)–H(2′*)···O(4′)(A5)). H–C(5′*)(A*) and H–C(1′)(A*) are only 2.6 Å apart, whereas the H–C(3′*)(A*) and H–C(1′)(A*) are separated by 4.4 Å. The H–C(1′*)(A*) points to the next A5 and is only 4.1 Å away from H–C(8)(A5). The O(2′)–C(1′*)–C(2′*)–O(2′*) torsion angle is –134° (dashed red arc).

range. These H-bonds probably drive the extra sugar ring into a well-defined orientation.

As this study was being completed, X-ray crystallography studies of related modified RNA duplexes containing 2′-*O*-(methoxyethyl) and 2′-O-(ethoxymethyl) modifications appeared, giving rationales for the observed increase in T_m for these molecules [3]. Increase in T_m can be achieved only if the two O-atoms in the alkoxyalkyl side chain are separated by an ethylene spacer, giving rise to a *gauche* conformation between these two O-atoms. In this conformation, a new hydration site is formed whereby a H_2O molecule interacts with both O-atoms of the side chain and also with O−C(3′) of the backbone sugar moiety. With the ethoxymethyl group, the spacing is wrong for an additional hydration. These results are supported by recent molecular-dynamics simulations [27] which suggest that H_2O molecules may help stabilize the *gauche* conformation, thus generating an electrostatic groove in the duplex that does not disturb the H_2O shell. In this study with the ribofuranosyl substituent, the O(2′)−C(1′*)−C(2′*)−O(2′*) torsion angle (−134°) does not have the *gauche* conformation (*Fig. 5*,*a*), responsible for the enhanced stability of the 2′-*O*-(methoxyethyl) derivatives. This result may partially explain the lack of an effect on stability due to the extra ribofuranosyl group, and hence the lack of a change in the observed melting temperature.

Besides the possible H-bonding as shown in *Fig. 5*,*b*, the H_2O structure may also play a crucial role in positioning the extra ribofuranosyl group and, therefore, we have performed molecular-dynamics simulations on the RNA duplex in H_2O. Although limited in their scope, these simulations showed that it was not possible to create a H_2O-mediated interaction between O(2′) and O(2′*) of the extra ribofuranose moiety and O−C(3′) of the backbone ribose moiety. The position of the extra ribofuranosyl substituent appeared to be stabilized by bridged H-bonds (mediated by two H_2O molecules) to the backbone of the complementary chain. These interactions involved one or both of the atoms O(3′*) and O(5′*) of the extra ribofuranosyl substituent, but the exact geometry of the interactions and the particular atoms involved in the complementary chain varied during the course of the simulations.

The extra ribose moiety disrupts the H-bonding between O(2′) of that residue and O(4′) of the next residue. However, our H_2O simulations also showed that it was possible to compensate for the loss of this H-bond by formation of a H-bond between O(2′*) and a H_2O molecule.

Conclusions. – The NMR data, represented by the measured NOEs and coupling constants, are consistent with the values found for an *A*-form double helix with all ribose residues (including the ribosyl substituent of the disaccharide nucleotide) adopting a C(3′)-*endo* (*N*-type) conformation. The extra ribofuranosyl unit of the disaccharide nucleotide occupies a well-defined position in the minor groove (*Fig. 5*), probably driven by H-bonding as shown in *Fig. 5*,*b*. Simulations incorporating H_2O suggested that bridged H-bond interactions with the complementary strand may be additionally responsible for defining the orientation of the extra ribofuranosyl unit. The conformation of the extra ribose unit is characterized by an O(2′)−C(1′*)−C(2′*)−O(2′*) torsion angle of −134° (*Fig. 5*,*a*). This means that the atoms O(2′) and O(2′*) are not positioned in the *gauche* relationship that was necessary

for the enhanced stability of RNA duplexes containing 2′-*O*-(methoxyethyl) modifications. Consequently, the typical hydration site found in the 2′-*O*-(methoxyethyl)-RNA is not present in the 2′-*O*-ribosyl congener. The fixed orientation of the extra ribose unit is such that it does not influence duplex stability in either a positive or negative way. Our NMR data are in agreement with the X-ray data [6], but we could also define the exact position of the individual atoms of this 2′-*O*-ribose moiety. This study will be followed by an analysis of the T-stem of a $tRNA_i^{Met}$ containing the 5′*-*O*-phosphorylated analogue of A*.

This work was supported by a grant from the *Onderzoeksfonds K. U. Leuven* (GOA 97/11). *Ingrid Luyten* thanks the *F.W.O.* for a fellowship. We thank *R. Busson* and *E. Lescrinier* for the NMR technical support and *Guy Schepers* for determining the melting temperatures.

REFERENCES

[1] P. Martin, *Helv. Chim. Acta* **1995**, *78*, 486.
[2] S. M. Freier, K. H. Altmann, *Nucl. Acids Res.* **1997**, *25*, 4429.
[3] V. Tereshko, S. Portmann, E. C. Tay, P. Martin, F. Natt, K. H. Altmann, M. Egli, *Biochemistry* **1998**, *37*, 10626.
[4] J. Desgrés, G. Keith, K. C. Kuo, C. W. Gehrke, *Nucl. Acids Res.* **1989**, *17*, 865.
[5] S. Kiesewetter, G. Ott, M. Sprinzl, *Nucl. Acids Res.* **1990**, *18*, 4677.
[6] R. Basavappa, P. B. Sigler, *EMBO J.* **1991**, *10*, 3105.
[7] P. V. Sahasrabudhe, R. T. Pon, W. H. Gmeiner, *Biochemistry* **1996**, *35*, 13597.
[8] E. V. Efimtseva, B. S. Ermolinsky, M. V. Fomitcheva, S. V. Meshkov, N. S. Padyukova, S. N. Mikhailov, J. Rozenski, A. Van Aerschot, P. Herdewijn, *Coll. Czech. Chem. Commun*. **1996**, *61*, S206.
[9] D. J. States, R. A. Haberkorn, D. J. Ruben, *J. Magn. Res.* **1982**, *48*, 286.
[10] F. Delaglio, S. Grzesiek, G. Vuister, G. Zhu, J. Pfeifer, A. Bax, *J. Biomol. NMR* **1995**, *6*, 277.
[11] T. Xia, C. Bartels, 'XEASY 1994', Institute of Molecular Biology and Biophysics, Zürich, Switzerland.
[12] P. Plateau, M. Guéron, *J. Am. Chem. Soc*. **1982**, *104*, 7310.
[13] M. Rance, O. W. Sørensen, G. Bodenhausen, G. Wagner, R. R. Ernst, K. Wüthrich, *Biochem. Biophys. Res. Commun*. **1983**, *117*, 479.
[14] A. Bax, D. G. Davies, *J. Magn. Res.* **1985**, *65*, 355.
[15] J. Jeener, B. H. Meier, P. Bachman, R. R. Ernst, *J. Chem. Phys*. **1979**, *71*, 4546.
[16] C. Griesinger, G. Otting, K. Wüthrich, *J. Am. Chem. Soc*. **1988**, *110*, 7870.
[17] V. Sklenar, H. Miyashiro, G. Zon, H. T. Miles, A. Bax, *FEBS Lett*. **1986**, *208*, 94.
[18] I. L. Barsukov, L.-Y. Lian, in 'NMR of Macromolecules. A Practical Approach', Ed. G. Roberts, Oxford University Press, New York, 1993, p. 315.
[19] S. S. Wijmenga, M. W. Mooren, C. W. Hilbers, in 'NMR of Macromolecules. A Practical Approach', Ed. G. Roberts, Oxford University Press, New York, 1993, p. 217.
[20] A. T. Brügner, 'X-PLOR. A System for X-Ray Crystallography and NMR', Yale University Press, New Haven, CT, 1992.
[21] E. G. Stein, L. M. Rice, A. T. Brügner, *J. Magn. Reson*. **1997**, *14*, 51.
[22] a) R. Lavery, H. Sklenar, *J. Biomol. Struct. Dynam*. **1988**, *6*, 63; b) R. Lavery, H. Sklenar, *J. Biomol. Struct. Dynam*. **1989**, *6*, 655.
[23] T. E. Ferrin, C. C. Huang, L. E. Jarvis, R. Landgridge, *J. Mol. Graph.* **1988**, *6*, 13.
[24] R. Sayle, E. James Milner-White, *Trends. Biochem. Sci.* **1995**, *20*, 374.
[25] R. M. Esnouf, *J. Mol. Graph. Modell.* **1997**, *15*, 132; D. J. Bacon, W. F. Anderson, *J. Mol. Graph*. **1988**, *6*, 219; E. A. Merritt, M. E. P. Murphy, *Acta Crystallogr., Sect. D* **1994**, *50*, 869.
[26] F. H.-T. Allain, G. Varani, *J. Mol. Biol*. **1995**, *250*, 333; C. W. Hilbers, S. S. Wijmenga, H. Hoppe, H. A. Heus, in 'NMR of Biological Systems', Ed. O. Jardetzky, Wiley, New York, 1996, pp. 193–207.
[27] K. E. Lind, V. Mohan, M. Manoharan, D. M. Ferguson, *Nucl. Acids Res.* **1998**, *26*, 3694.

Received February 25, 2000